4ICEGE Thessaloniki-GREECE 2007

4th International Conference on
Earthquake Geotechnical Engineering
June 25-28, 2007
Paper No. 1569

SEISMIC TRIGGERING, EVOLUTION AND DEPOSITION OF MASSIVE LANDSLIDES. THE CASE OF HIGASHI−TAKEZAWA (2004)

Nikos GEROLYMOS[1], George GAZETAS[2]

ABSTRACT

In the October 2004 Niigata-Ken Chuetsu M_{JMA} = 6.8 earthquake more than 1600 landslides have been reported. Among them of particular interest is the Higashi–Takezawa landslide, which involved 100 m displacement of a large wedge of an originally rather mild slope. One of the mysteries of the landslide is the exact location of the sliding surface. The goal of the paper is to study: (i) the landslide triggering and propagation, and (ii) the mechanism of material softening inside the shear band responsible for the accelerating movement of the slide. A model is presented considering two mechanically coupled substructures: (a) the accelerating deformable body of the slide, and (b) the rapidly deforming shear band at the base of the slide. It combines features of an extended Savage–Hutter approach, with (a) Mohr–Coulomb failure criteria, (b) Bouc–Wen hysteretic stress–strain relationship, and (c) grain crushing–induced pore–water pressures model (Gerolymos and Gazetas, 2007). The method successfully interprets the studied landslide.

Keywords: Savage–Hutter model; grain crushing; seismic triggering; deposition; rapid landslide.

INTRODUCTION

The devastating 2004 Niigata–Ken Chuetsu earthquake (M_w 6.8) triggered 374 landslides more than 50 m wide (Sassa et al., 2005) 12 of which with volume larger than one million cubic meters. Among these landslides, Higashi–Takezawa was one of the largest. The landslide mass filled a valley and stopped a river flow forming a large natural reservoir. It is believed, however, that the heavy rainfall during the last three days before the earthquake was a significant contributor to the triggering of those landslides (Sassa 2005; Tsukamoto and Ishihara, 2005).

The surprisingly large and rapid runoff of the soil mass motivated several researchers (Kokusho and Ishizawa, 2005; Tsukamoto and Ishihara, 2005, Sassa et al., 2005) to study the Higashi–Takezawa landslide, providing different interpretations of the sliding process. The questions to be answered arose on: (a) the exact position of the sliding surface, and (b) the mechanism of material softening behind the accelerating landslide movement. It is pointed out, that laboratory tests on soil samples taken from the site of the slip surface indicated undrained friction angles larger than the slip inclination (Sassa et al., 2005). Moreover, the sliding material consisting of silt to dense silty sand was not susceptible to liquefaction (Kokusho and Ishizawa, 2005).

Sassa (1994; 1995) developed the theory of sliding surface liquefaction to explain the rapid evolution of earthquake–induced landslides. The theory was experimentally supported by undrained loading ring shear tests simulating the actual conditions (Sassa et al., 1996; 2004). It was shown that grain crushing–induced liquefaction may occur not only in fully water–saturated soils (Sassa et al., 2005), as

[1]Lecturer, School of Civil Engineering, National Technical University, Athens, Greece, Email: gerolymos@mycosmos.gr
[2]Professor, School of Civil Engineering, National Technical University of Athens, Greece, Email: gazetas@ath.forthnet.gr

is usually the case for mass liquefaction, but also in partially saturated soils (Sassa et al., 1996). The theory was successfully used to describe the evolution of rapidly moved landslides, in the Hyogoken-Nambu 1995 earthquake: the Nikawa and Takarazuka landslides (Sassa et al., 1996), and in the Niigata–Ken Chuetsu 2004 earthquake: the Higashi Takezawa and Terano landslides (Sassa et al., 2005).

After a detailed field survey of the head scarp of the Higashi–Takezawa landslide, Sassa et al. (2005) concluded that the sliding surface could have been formed within either the weathered (due to the existence of groundwater flow) top part of the outcropped siltstone layer, or the bottom of the overlain sand layer which was probably a part of previously moved landslide mass. Ring shear tests conducted by Sassa et al. (2005) on soil specimens taken from the sliding surface revealed that the residual friction angle of the silt was by far smaller than that of the sand, and close to the inclination angle of the slip plane. Neither of them could explain the rapid and large displacement of the landslide. However, the sand was found to be susceptible to grain–crushing induced liquefaction exhibiting an apparent friction angle of 3.3^{o}. These findings lead Sassa et al. (2005) to the following interesting conclusions: Landslide should occur in the silt layer when long rain or melting snow is the triggering factor, since it is certain that silt is much weaker than the sand. In contrast, the silt is strong against earthquake, while sand grains are crushable and susceptible to volume reduction. Therefore, earthquake induced landslide should form its sliding surface within the sand.

In the present study, a slope stability analysis for estimating the static factor of safety of the Higashi–Takezawa landslide is performed using the finite element method. Two cases are considered regarding the location of the sliding surface: (a) in the weathered top part of the outcropped siltstone layer, and (b) in the bottom of the sand layer above the siltstone. The factor of safety computed for both cases suggests the slope is stable even in strong earthquake loading. However, the potential sliding surface would be formed within the silt layer.

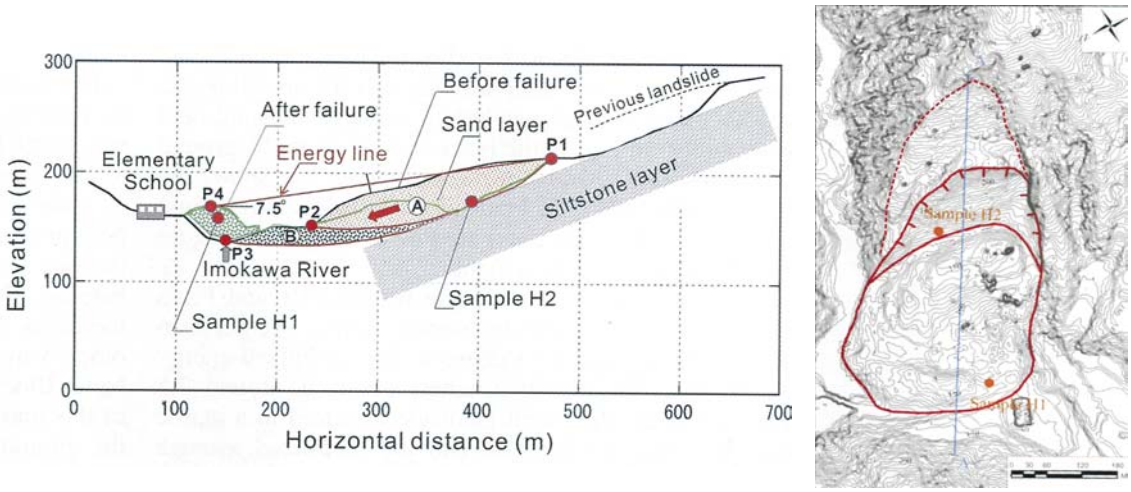

Figure 1. The Higashi–Takezawa landslide: (a) cross section, and (b) plan view (Sassa et al., 2005)

THE HIGASHI–TAKEZAWA LANDSLIDE

The main body of the landslide is indicated in the plan of **Fig 1** deduced from an air borne laser scanning survey (Sassa et al., 2005) carried out three days after the earthquake. A cross–section of the landslide is also depicted in **Fig 1**. The gentle slope inclination before the head scarp reveals that the landslide was a reactivation of a previous one. The landslide involved a soil volume of about 1 200 000 m^3 (Kokusho and Ishizawa, 2005). The maximum dimensions in plan were about 300 m width and 250 m length (Kokusho and Ishizawa, 2005), and the maximum thickness was about 40 m (Sassa et al., 2005). The landslide mass moved rapidly around 100 m, and hit the opposite bank of Imokawa

river (Sassa et al., 2005). A part of the sliding mass spread across the road and hit a school. From the head scarp of the landslide, consisting of a rather impermeable stiff siltstone, the inclination angle of the sliding surface was estimated to be approximately 20^o (Sassa et al., 2005; Kokusho and Ishizawa, 2005).

A schematic geological section of the landslide area is shown in **Fig 1**. The subsoil is essentially constituted of a Neogene formation, consisting of sandstone (the main body of the landslide) underlain by siltstone. The terrace along the river and below the toe of the landslide consists of marine sand from the Tertiary period (Sassa et al., 2005). The groundwater flow over the siltstone layer, lead Sassa et al. (2005) to assume the existence of a thin silt layer between the sandstone and the siltstone, due to weathering of the siltstone. Although, this silt layer was not detected at the head scarp, the assumption of Sassa et al. (2005) was reinforced from field investigation of the head scarp of the Terrano landslide located in the vicinity of Higashi–Takezawa and near the Immokawa river. The Terrano landslide (Sassa et al., 2005), was also triggered by Niigata–Ken Chuetsu earthquake, and had the same subsoil and groundwater conditions. The silt encountered at the head scarp of the Terrano landslide was well weathered and soft.

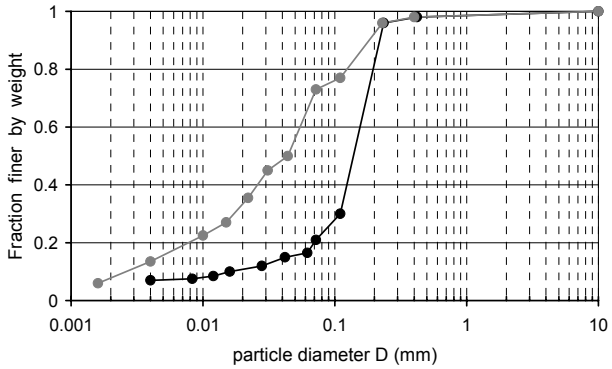

Figure 2. Grain size distribution of the Higashi–Takezawa sand (black line) and Terrano silt (gray line), after Sassa et al. (2005)

Water seepage observed on the head scarp of the landslide three days after the earthquake suggests that the water table was located well above the sliding plane. No precipitation was observed during a period of several days preceding the earthquake, which occurred during the rainy season.

The grain size distribution of the sand involved in the sliding surface of the Higashi–Takezawa landslide is illustrated in **Fig 2**, along with that of the Terrano silt which is considered to be representative of the Higashi–Takezawa one. The strength properties of the soils under consideration were obtained from consolidated–drained and undrained high speed ring shear tests (Sassa et al., 2005). The undrained friction angle of the sand was found to be 36.9^o, while the residual friction angle of the Terrano silt was 23.9^o. However, one peculiar aspect of the Higashi–Takezawa sand is its mechanical instability due to grain crushing. The cyclic loading test, resulting in an apparent friction angle of 3.3^o, indicated that the Higashi–Takezawa sand is susceptible to grain crushing–induced liquefaction.

FINITE ELEMENT ANALYSIS OF SLOPE STABILITY

The finite element model (**Fig 3**) refers to the geological section of **Fig 1**. The analysis is performed using the code PLAXIS (Brinkgreve and Vermeer, 1998). The soil behaviour is described by an elastic perfectly plastic Mohr–Coulomb failure criterion with non–associated plastic flow rule. Due to lack of specific experimental results, estimation of Young's modulus E, Poisson's ratio v, for all soils involved in the analysis, and strength parameters φ' (effective internal friction angle) and ψ (dilatancy angle) for the marine sand, was based on engineering judgement. However, the actual

values of those parameters would only slightly affect the results. The dilatancy angle of the sand and the silt is assumed to be nil, implying deformation with zero volume change during yield. The groundwater level is estimated based on the field observations of Sassa et al. (2005). Two cases are analyzed regarding the location of the failure surface: (a) within the sand layer, and (b) within an assumed thin silt layer at the top of the siltstone. The results of the analysis are shown in **Fig 4** in terms of displacement vectors plotted on the deformed finite element mesh. The factors of safety were computed to be 2.5 and 1.9 for the first and the second case, respectively. Therefore, one could reasonably assume that the potential sliding surface due to strong earthquake loading would be formed within the silt layer.

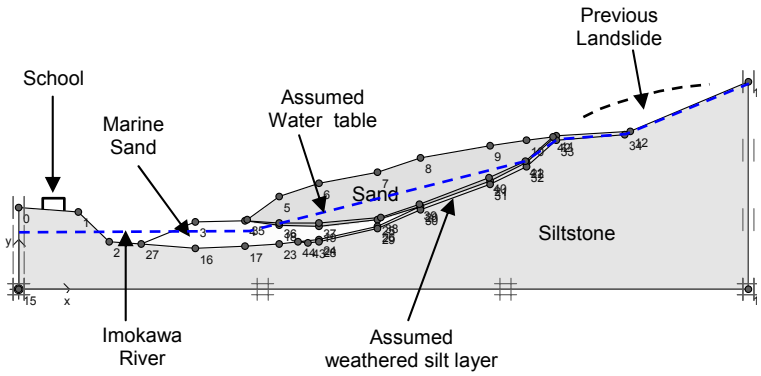

Figure 3. Geometry and geological characteristics of the finite element model used in the slope stability analysis of Higashi–Takezawa

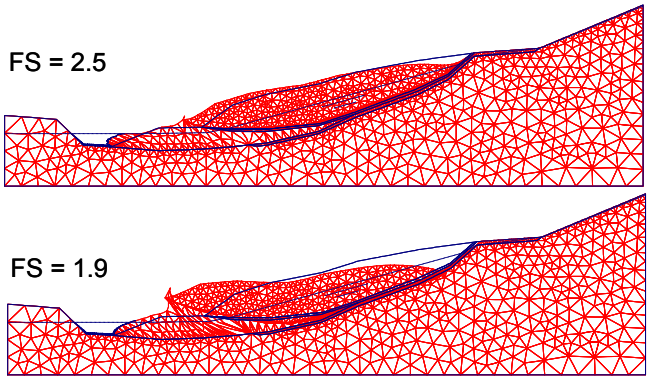

Figure 4. Deformed finite element mesh of the Higashi–Takezawa landslide at the beginning of failure. Failure surface: (a) within the sand layer, and (b) within an assumed thin silt layer at the top of the siltstone. The factors of safety were computed to be 2.5 and 1.9 for the first and the second case, respectively

THE MODEL : EQUATIONS AND PARAMETERS

Problem definition

The problem studied is that of a finite moving soil mass assembled by a number of columns in contact with each other. The columns are free to deform but retain fixed volumes (constant density ρ_s) of solid–fluid mixtures during their movement down a slope. The evolution of the mixture is considered to be one–dimensional with no aggradation or degradation processes and with uniformly–distributed (depth–integrated) velocity along each column. At the base of the sliding mass we assume a shear band of infinite length and of zero thickness.

The field variables are the thickness of the landslide h, excess pore water pressure p, the breakage potential B_p, and the relative velocity υ between top and bottom. The landslide thickness, and pore water pressure are assumed to be function of time, t, and of the local coordinate, x, whereas the rate of particle breakage is only a function of time. The velocity is considered to increase linearly with the distance from the bottom of the shear band, from zero to the maximum value υ at the top of the shear band; υ is also considered a function solely of time. The breakage potential B_p is a measure of the evolution of the particle size distribution curve with loading, as defined in the sequel. It is pointed out that the parameter B_p is the current value of the breakage potential, and should not be confused with that originally defined by Hardin (1985), denoted as B_{p0}. The latter, B_{p0}, is the initial (i.e. before loading) breakage potential and is a constant.

Applying the mass and momentum conservation laws and using Eulerian description of motion, a system of two partial differential equations are obtained:

$$\frac{\partial h}{\partial t} + \upsilon \frac{\partial h}{\partial x} + h \frac{\partial \upsilon}{\partial x} = 0 \tag{1}$$

and

$$\frac{\partial \left(h \bar{\sigma}_x \right)}{\partial x} + T_d - T_r - T_f = \rho_s h \left(\frac{\partial \upsilon}{\partial t} + \upsilon \frac{\partial \upsilon}{\partial x} + \frac{d \upsilon_g}{dt} \right) \tag{2}$$

h is the thickness in the z direction normal to the bed, υ is the depth–averaged velocity in the x direction parallel to the base of the landslide, υ_g is the seismic acceleration imposed at the base of the landslide parallel to the dip direction of the sliding surface, T_d is the gravitational driving force acting on the landslide mass, T_r is the resisting force due to hysteretic (Coulomb) friction at the bed influenced by bed curvature (Gray et al. 1999, Iverson and Delinger 2001, Pudasaini and Hutter, 2003); It is a function of τ_m the cyclic shear resistance mobilized along the shear band. A detailed description of this term will be provided below; and T_f the turbulent resisting force at the base of the slide, represented by the quadratic Chezy constitutive law.

In Eqn (2), $\bar{\sigma}_x$ is the average – along the depth of the sliding mass – longitudinal normal stress due to elongation or compression of the soil mass in the x direction. The longitudinal normal stress is assumed to be a combination of a lithostatic (depth–dependent) term and a strain rate dependent term

$$\bar{\sigma}_x = \frac{1}{2} \left(K - \frac{2 \eta_d}{g \cos\theta} \frac{\partial \upsilon}{\partial x} \right) \rho_s g h \cos\theta \tag{3}$$

in which K is the lateral earth pressure coefficient at rest, and η_d is a coefficient that determines the magnitude of the horizontal normal stress at yielding. It could be in the active ($\partial \upsilon / \partial x > 0$) or in the passive ($\partial \upsilon / \partial x \leq 0$) state, depending on whether a soil column is expanding or contracting. For the special case of $K = 0$ and $\eta_d = 0$, the sliding mass behaves as a rigid body and Eqn (2) vanishes to the well known Newmark sliding block model.

Equations for frictional behaviour

A versatile one–dimensional constitutive model is utilised to describe the shear stress–displacement relationship inside the shear band. The model is capable of reproducing an almost endless variety of stress–strain forms, monotonic as well as cyclic. Based on the original proposal by Bouc (1971) and Wen (1976), the model was recently extended by Gerolymos and Gazetas (2005) and applied to cyclic response of soils and earthquake–triggered rapid landslides (Gerolymos et al., 2007;

Gerolymos and Gazetas, 2007). It is used herein in conjunction with a Mohr–Coulomb friction law and Terzaghi's effective stress principle.

The mobilized shear stress inside the shear band is expressed as:

$$\tau_m = \tau_y \zeta \tag{4}$$

where τ_y is the ultimate shear strength, which is a function of time. The parameter ζ is a hysteretic dimensionless quantity, controlling the nonlinear response of the soil. It is governed by the following differential equation:

$$\frac{d\zeta}{du} = \frac{1}{u_y}\left\{1 - |\zeta|^n \left[b + (1-b)\,\mathrm{sgn}(\upsilon\zeta)\right]\right\} \tag{5}$$

in which u_y , n and b, are parameters that control the shape of the shear stress versus displacement curve. The parameter τ_y is defined as:

$$\tau_y = \mu(\sigma'_{n0} - p) \tag{6}$$

in which the friction coefficient, μ, is expressed in terms of the Coulomb friction angle φ' of the soil in direct shear, σ'_{n0} is the initial effective normal stress, and p is the excess pore–water pressure, generated due to particle breakage.

Equations for grain crushing–induced pore–water pressure

The mechanism of pore–water pressure generation due to particle breakage is assumed to be governed by the following equation (Gerolymos and Gazetas, 2007):

$$\frac{\partial p}{\partial t} + \upsilon\frac{\partial p}{\partial x} = \frac{\partial}{\partial z}\left(c_v(B_p)\frac{\partial p}{\partial z}\right) - \lambda\frac{\partial B_p}{\partial t}\sigma'_{n0} \tag{7}$$

in which B_p is the current value of the breakage potential; c_v and λ are the coefficients of consolidation and pore–pressure–breakage, respectively. Note that c_v is a function of B_p. In fact, c_v decreases with decreasing particle size and thus with particle crushing evolution.

This expression is being simplified in the limit of undrained loading conditions, which is a reasonable assumption when the shear band is deformed at a large velocity (rapid landslide). Parameter λ controls the ultimate value of the pore–water pressure. The larger the value of λ, the higher the asymptotic value of the pore–water pressure.

Equations for grain crushing

As already discussed, the breakage potential B_p is a measure of the evolution of the particle size distribution curve with loading, and hence of the amount of grain crushing. We assume that the evolution of B_p with time is governed by the following equation (Gerolymos and Gazetas, 2007):

$$\frac{dB_p}{dt} = \xi(B_{pl} - B_p) \tag{8}$$

in which B_{pl} is the final (after loading) breakage potential as computed at the current time of loading, given by:

$$B_{pl} = \frac{B_{p0}}{1 + S^{n_b}} \tag{9}$$

in which B_{p0} is the initial (before loading) value of B_p, defined as (Hardin, 1985). The definition of B_{p0} is schematically illustrated in **Fig 5**. The breakage number, n_b, is expressed as a function of the crushing hardness h_c , shape number of the particle n_s , and the initial void ratio e_0 of the particles mixture (Hardin, 1985). The stress loading factor S is a function of both the mobilized shear stresss τ_m , and the effective normal stress σ'_n (Hardin, 1985; Gerolymos and Gazetas, 2007).

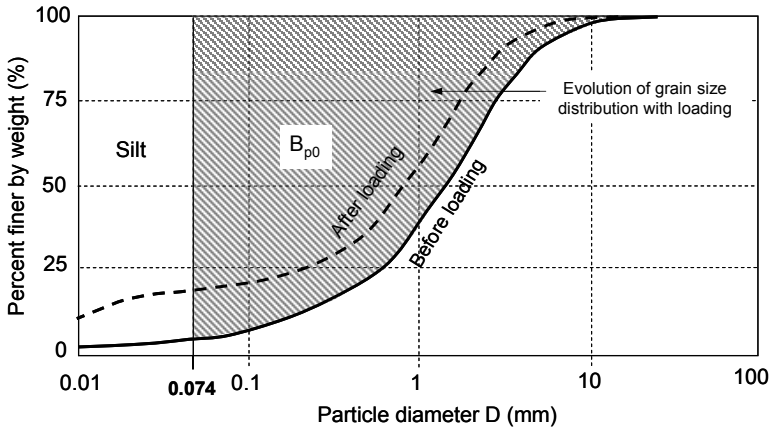

Figure 5. Definition of the initial breakage potential B_{p0}, after Hardin (1985)

For a given shear stress time history, Eqns (4), (5), (7), and (8) form a system of highly nonlinear partial differential equations with four unknowns: the excess pore–water pressure p, the breakage potential B_p, the hysteretic parameter ζ, and the displacement u.

Numerical formulation and calibration of model parameters

An explicit finite difference technique is used for the solution of Eqns (1) and (2), which are coupled with the constitutive Eqns (5), (7), and (8) and the appropriate equations for boundary and initial conditions, providing the necessary coupling between the two substructures (the deformable soil body, and the shear band). Calibration of the parameters for shear band behaviour is achieved through numerical simulation of undrained cyclic ring shear tests conducted by Sassa et al. (2005). The shape number, crushing hardness, and initial void ratio were assumed to be n_s = 25, h_c = 2.4, and e_0 = 0.6, respectively, while the initial breakage potential was calculated from **Fig 2** to B_{p0} = 0.34. Detailed information on the aforementioned parameters is given by Hardin (1985).

The experimental results are reproduced in **Figs 6** in the form of time history of the developed shear displacement, and plot of the shear resistance versus effective normal stress. The breakage and pore–pressure breakage coefficients correspond to the analysis are ξ = 0.05 and λ = 25. Note that the proposed model is capable of reproducing the brittle behaviour of a soil undergoing grain crushing–induced pore–pressure. That is, loss of shear resistance occurs only after the yield surface has been reached, by contrast to conventional (mass) liquefaction in which degradation of shear resistance initiates below the yield surface, when the phase transformation line has been reached.

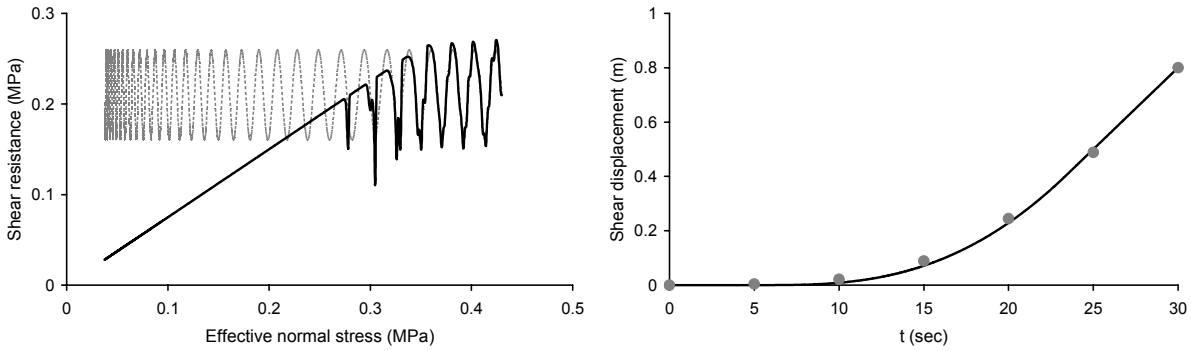

Figure 6. (Left) Computed stress path of the undrained cyclic ring shear test on the Higashi–Takezawa sand (the loading is plotted with gray line). (Right) Computed time histories of shear displacement of the undrained cyclic ring shear test of the Higashi–Takezawa sand [the circles correspond to the experimental data of Sassa et al. (2005)]

RESULTS AND CONCLUSION

With the developed model for seismic triggering and evolution of grain–crushing–induced landslide we analyse the case of Higashi–Takezawa. The parameters are: ρ_s = 2 t / m^3, K = 0.5, η_d = 5, μ_T = 0.01h, n = 3, b = 0.5, $u_y = 10^{-3}$ m, μ = 0.75, n_s = 25, h_c = 2.4, e_0 = 0.6, B_{p0} = 0.34, λ = 25, and ξ = 0.05. The seepage force is ignored, since the actual level of the water table during the earthquake is not known. The actual seismic excitation exerted on the landslide cannot be known in detail, as it is influenced by many parameters such as the geology, topography, site conditions and distance from the fault. Therefore, we apply as excitation the EW–component of the record from the nearest (to the landslide) observation station NIG019 at Ojiya (PGA = 1.3 g), around 10 km west of the Higashi–Takezawa landslide and WNW 7 km from the epicenter of the main shock (Sassa et al. 2005). Three scenarios are studied regarding the potential location of the sliding surface and the susceptibility of sand to grain crushing:

(a) The shear band formed within the sand layer (i.e., in the main body of the landslide), the sand is not susceptible to grain crushing, and the upper part of the siltstone is assumed to have remained intact.

(b) The shear band formed within an assumed thin silt layer atop the siltstone, but the sand is not susceptible to grain crushing.

(c) The shear band formed within the sand layer, the sand *is* susceptible to grain crushing, and the upper part of the siltstone is assumed to have remained intact.

The results of the analysis for cases (a) and (b) are shown comparatively in **Fig 7** in the form of time histories of relative shear displacement. The maximum computed displacement at the end of shaking for case (a) is 0.65 m, which is by far smaller than that of 3.4 m for case (b). These values of displacement are both consistent with the static factors of safety calculated from the slope stability analysis (FS = 1.9 and 2.5 for the shear band within the silt and the sand layer, respectively), suggesting that the existence of a thin silt layer atop the siltstone is more crucial for triggering the landslide. However, none of those displacements could explain the observed rapid and large run-out distance of the landslide. It is therefore reasonable to assume that grain crushing–induced pore–pressures could be a major destabilizing factor for the landslide.

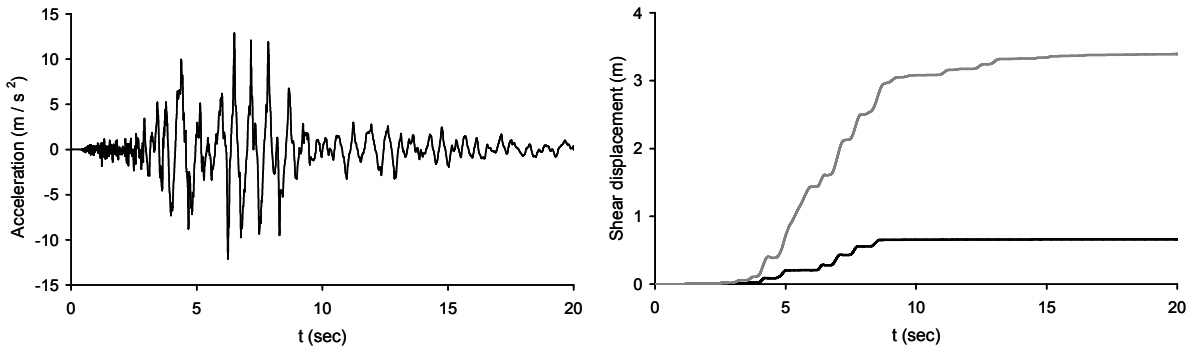

Figure 7. (Left) Input acceleration time history (NIG019–EW 2004 - PGA = 1.3 g) at the base of the landslide. (Right) Computed time histories of relative shear displacements, for sliding surface: (i) within the sand layer(no grain crushing is considered, max*u* = 0.65 m) (black line), and (ii) within an assumed thin silt layer at the top of the siltstone (max*u* = 3.4 m) (gray line)

The results of the analysis for case (c) are presented in **Fig 8** in terms of snapshots of the landslide evolution (**Fig 8a**), and distributions of velocity v (**Fig 8b**), excess pore–water pressure ratio r_u (**Fig 8c**), and breakage potential B_p (**Fig 8d**), along the sliding surface. The following observations are worthy of note regarding the response of the sliding wedge:

At the early stages of the seismic motion, excess pore water–pressure due to particle crushing is generated at the head of the wedge and propagates rapidly towards its toe. In the following few seconds the excess pore–water pressure ratio rises up very quickly reaching values larger than 0.9 along the entire length of the sliding surface (t = 12.5 sec – blue line). At this time, sliding originates at the head of the soil wedge, and landsliding begins. It is very interesting that triggering occurs almost at the end of seismic shaking, when the motion has essentially subsided, and not during the strong seismic shaking as one would expect. This implies that grain crushing–induced pore–pressure is a cumulative process and thus depends strongly on the history of loading.

After its initiation the landslide moves rapidly towards the riverbed, developing velocities between 5 m/s and 16 m/s. Velocities with smaller values concentrate on the rear of the landslide, while those with larger values are mostly at the front which essentially governs the "race" of the entire landslide. At t = 22.5 sec the sliding soil mass enters the riverbed while at this time the frontal part of the landslide detaches from the main body, spreads across the river, hits the opposite bank with a velocity of 25 m / s (at t = 26.5 sec), and finally reaches the school at t = 30 sec. Following this frenetic motion of the detached frontal part, the main body of the landslide accumulates inside the riverbed forming a natural reservoir which decelerates the trailing part of the landslide. The reduction in velocity begins at the rear and progressively shifts to the front.

It is seen that the calculated sliding process extended from the ruptured scrap in the source zone to the deposition fan on the riverbed and near the school, is consistent with the field observation (Sassa et al., 2005). Clearly, there are four major stages in the run-out process, namely, triggering (at t ≈ 12.5 sec), accelerating motion towards the riverbed (12.5 sec < t < 22.5 sec), separation of the frontal part from the main body of the landslide (at t = 22.5 sec), and deposition and deceleration (t > 22.5 sec).

To get an insight into the mechanics behind this disastrous response, **Fig 8d** plots the evolution of particle breakage potential B_p. Notice that B_p approaches a steady state value of 0.30 at t > 15 seconds; this is larger than the initial value of B_{pl} (computed to be 0.27 in drained loading conditions), reflecting the influence of the developed excess pore–water pressures. The slightly increasing breakage potential at t > 15 seconds reveals that the grain crushing process has been practically terminated. The effective normal stress is not adequate for further breakage. However, the landslide is still accelerating due to the action of gravity.

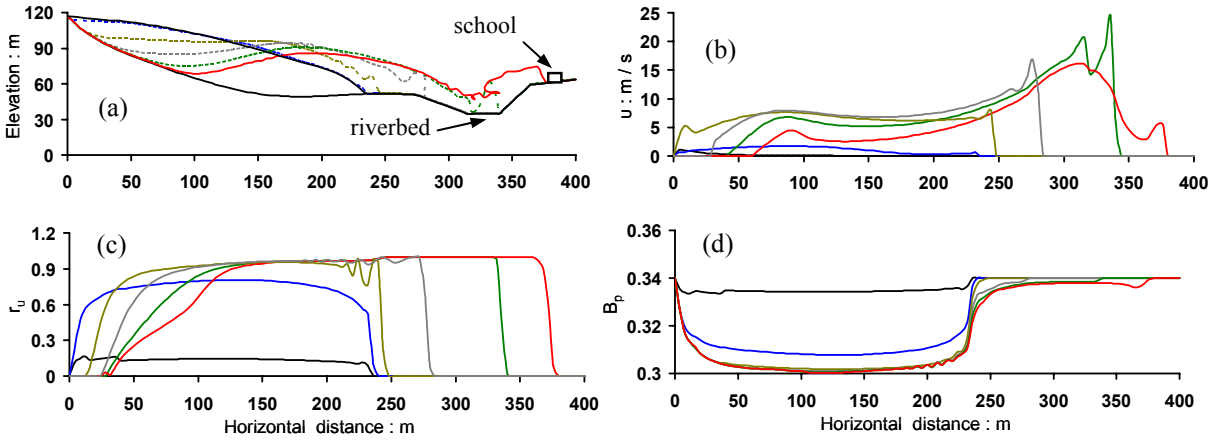

Figure 8. (a) Snapshots of the landslide evolution, and distributions along the sliding surface of (b) velocity, (c) excess pore–water pressure ratio r_u, and (d) breakage potential B_p , at t = 5 sec (black line), t = 12.5 sec (blue line), t = 19 sec (golden line), t = 22.5 sec (gray line), t = 26 sec (green line), and t = 30 sec (red line)

ACKNOWLEDGMENTS

This paper is a partial result of the Project PYTHAGORAS I / EPEAEK II (Operational Programme for Educational and Vocational Training II) [Title of the individual program: Mathematical and experimental modeling of the generation, evolution and termination mechanisms of catastrophic landslides].This Project is co-funded by the European Social Fund (75%) of the European Union and by National Resources (25%) of the Greek Ministry of Education.

REFERENCES

Brinkgreve R B J, Vermeer P A (1998) PLAXIS finite elements code for soil and rock analysis, Version 7.2. Rotterdam: Balkema.

Chang K J, Taboada A, Lin M-L, Chen R-F (2005) “Analysis of landsliding by earthquake shaking using a block-on-slope thermo-mechanical model: Example of Jiufengershan landslide, central Taiwan”. Engineering Geology 80: 151-163.

Gerolymos N, Gazetas G (2005) “Constitutive Model for 1-D Cyclic Soil Behavior Applied to Seismic Analysis of Layered Deposits”. Soils and Foundations 45(3): 147–159.

Gerolymos N, Gazetas G (2007) “A Model for Grain Crushing Induced Landslides − Application to Nikawa, Kobe 1995”. Soil Dynamics and Earthquake Engineering (accepted for publication).

Gerolymos N, Vardoulakis I and Gazetas G. (2007) “A thermo-poro-viscoplastic shear band model for triggering and evolution of catastrophic landslides”. Soils and Foundations 47(1).

Gray J.M.N.T., Wieland M., Hutter K. (1999) “Gravity driven free surface flow of granular avalanches over complex topography, Proc. R. Soc. London A 455, 1841-1874.

Hardin B (1985) “Crushing of Soil Particles”. Journal of Geotechnical Engineering 111(10): 1177-1192.

Iverson R. M., Delinger R. P. (2001) “Flow of variably fluidized granular masses across three-dimensional terrain. 1. Coulomb mixture theory, J. Geophys. Res. B, 106, 537-552.

Kokusho T, Ishizawa T (2005) “Energy approach to slope failures and a case study during 2004 Niigata–ken Chuetsu earthquake”. Proceedings of Geotechnical Earthquake Engineering Satellite Conference Osaka, Japan, 10 September 2005, Performance Based Design in Earthquake Geotechnical Engineering: Concepts and Research, ISSMGE: 255-262.

Pudasaini S. P., Hutter K. (2003) “Rapid shear flows of dry granular masses down curved and twisted channels, J. Fluid Mech., 495, 193-208.
Sassa K, Fukuoka H, Wang F, Wang G (2005) “Dynamic properties of earthquake-induced large-scale rapid landslides within past landslide masses”. Landslides 2: 125-134.
Sassa K (2005) “Landslide disasters triggered by the 2004 Mid-Niigata Prefecture earthquake in Japan”. Landslides 2: 135-142.
Sassa K, Fukuoka H, Wang G, Ishikawa N (2004) “Undrained dynamic–loading ring–shear apparatus and its application to landslide dynamics”. Landslides 1: 7–19.
Sassa K, Fukuoka H, Scarascia-Mugnozza G, Evans S (1996) “Earthquake induced Landslides: distribution, motion and mechanisms”. Special Issue of Soils and Foundations, Japanese Geotechnical Society: 53-64.
Sassa K (1995) “Keynote lecture: Access to the dynamics of landslides during earthquakes by a new cyclic loading high-speed ring shear apparatus”. Proceedings 6th International Symposium on Landslides 1992, In “Landslides”, Balkema 3: 1919-1939.
Sassa K (1994) “Development of a new cyclic loading ring shear apparatus to study earthquake–induced–landslides”. Report for Grant-in-Aid for Development Scientiffic Research by the Ministry on Education, Science and Culture, Japan (Project No. 03556021): 1-106.
Tsukamoto Y, Ishihara K (2005) “Residual strength of soils involved in earthquake–induced landslides”. Proceedings of Geotechnical Earthquake Engineering Satellite Conference Osaka, Japan, 10 September 2005, Performance Based Design in Earthquake Geotechnical Engineering: Concepts and Research, ISSMGE: 117-123.
Wen Y-K (1976) “Method for random vibration of hysteretic systems”. Journal of Engineering Mechanics, ASCE 102: 249-263.